The crystal structure of the bifunctional enzyme 6-phosphofructo-2-kinase/fructose-2,6-bisphosphatase reveals distinct domain homologies

Charles A Hasemann†*, Eva S Istvan[1], Kosaku Uyeda[1,2] and Johann Deisenhofer[1,3]

Background: Glucose homeostasis is maintained by the processes of glycolysis and gluconeogenesis. The importance of these pathways is demonstrated by the severe and life threatening effects observed in various forms of diabetes. The bifunctional enzyme 6-phosphofructo-2-kinase/fructose-2,6-bisphosphatase catalyzes both the synthesis and degradation of fructose-2,6-bisphosphate, a potent regulator of glycolysis. Thus this bifunctional enzyme plays an indirect yet key role in the regulation of glucose metabolism.

Results: We have determined the 2.0 Å crystal structure of the rat testis isozyme of this bifunctional enzyme. The enzyme is a homodimer of 55 kDa subunits arranged in a head-to-head fashion, with each monomer consisting of independent kinase and phosphatase domains. The location of ATPγS and inorganic phosphate in the kinase and phosphatase domains, respectively, allow us to locate and describe the active sites of both domains.

Conclusions: The kinase domain is clearly related to the superfamily of mononucleotide binding proteins, with a particularly close relationship to the adenylate kinases and the nucleotide-binding portion of the G proteins. This is in disagreement with the broad speculation that this domain would resemble phosphofructokinase. The phosphatase domain is structurally related to a family of proteins which includes the cofactor independent phosphoglycerate mutases and acid phosphatases.

Addresses: [1]Department of Biochemistry, University of Texas Southwestern Medical Center, 5323 Harry Hines Blvd., Dallas, TX 75235 USA, [2]Research Service, Department of Veterans Affairs Medical Center, 4500 S. Lancaster Rd., Dallas, TX, 75216 USA and [3]Howard Hughes Medical Institute, University of Texas, Southwestern Medical Center, 5323 Harry Hines Blvd., Dallas, TX 75235, USA.

†Present address: Department of Internal Medicine, Division of Rheumatology, and the Harold C Simmons Center for Arthritis Research, University of Texas Southwestern Medical Center, 5323 Harry Hines Blvd., Dallas, TX 75235-8884, USA.

*Corresponding author.
E-mail: hasemann@howie.swmed.edu

Key words: bifunctional enzyme, phosphoric monoester hydrolase, phosphotransferase, protein structure, X-ray crystallography

Received: 31 May 1996
Revisions requested: 28 June 1996
Revisions received: 15 July 1996
Accepted: 15 July 1996

Structure 15 Sept 1996, 4:1017–1029

Introduction

Glycolysis and gluconeogenesis in the liver are the primary processes responsible for maintenance of glucose homeostasis. The profoundly debilitating effects observed in diabetes mellitus underscore the importance of the accurate maintenance of these processes. The β anomer of fructose-2,6-bisphosphate (Fru-2,6-P_2) is a key regulatory molecule for glycolysis (and to some extent for gluconeogenesis) via its potent stimulatory effect on phosphofructokinase (PFK) activity and its inhibitory effect on fructose-1,6-bisphosphatase (Fru-1,6-P_2ase) [1–3]. 6-Phosphofructo-2-kinase (6-PF-2-K) synthesizes Fru-2,6-P_2 from fructose-6-phosphate (F6P) and ATP, while fructose-2,6-bisphosphatase (Fru-2,6-P_2ase) hydrolyzes Fru-2,6-P_2 to form F6P and inorganic phosphate (P_i). These antagonistic activities reside in a single bifunctional enzyme, 6-phosphofructo-2-kinase/fructose-2,6-bisphosphatase (6-PF-2-K/Fru-2,6-P_2ase), which is found in the cytosol of all tissues as a homodimer of ~56 kDa subunits. Homology of the C-terminal half of the 6-PF-2-K/Fru-2,6-P_2ase amino acid sequence with that of the yeast phosphoglycerate mutase [4], together with analysis of various truncated expression constructs [1,5,6], showed the enzyme to be divided into two functional domains. The N-terminal catalytic domain houses the 6-PF-2-K activity, and the C-terminal domain houses the Fru-2,6-P_2ase activity.

Five mammalian isozymes of 6-PF-2-K/Fru-2,6-P_2ase have been discovered to date (isolated from liver, skeletal muscle, heart, testis and brain,). The liver and skeletal muscle isozymes arise by alternative splicing of a single gene, while distinct genes encode the others [7–10]. The muscle isozyme has the shortest N terminus, but retains high 6-PF-2-K activity, and thus defines the N-terminal border of the functional 6-PF-2-K domain (Fig. 1). The other isozymes have N-terminal extensions which, in the liver and testis enzymes, modulate enzyme activity [11]. The heart enzyme exists in two forms, differing by a C-terminal extension which has a role in modulating the activity of the enzyme [12].

Figure 1

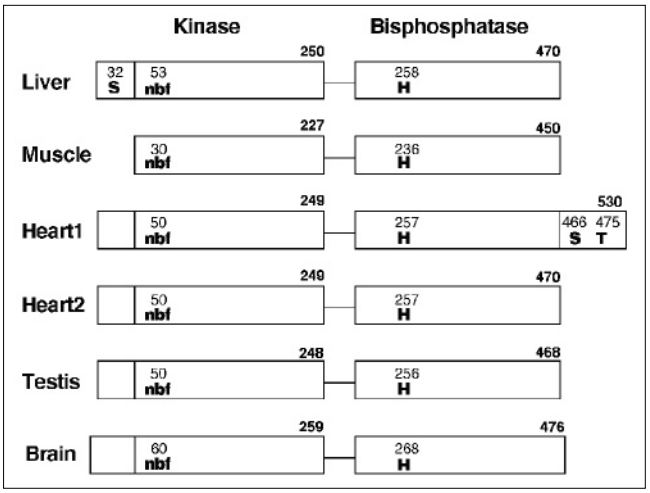

Domain diagrams of the mammalian 6-PF-2-K/Fru-2,6-P_2ase enzymes. Serine and threonine (S,T) residues which are phosphorylated are shown, as well as the location of the nucleotide-binding motif (nbf) in the kinase domain, and the catalytic histidine (H) in the phosphatase domain. The N-terminal extensions of the liver and testis isozymes and the C-terminal extension of the heart1 isozyme have been shown to modulate enzyme activity.

If the opposing activities of 6-PF-2-K/Fru-2,6-P_2ase were unregulated, this would lead to the futile cycling of substrates, and the unproductive expense of ATP. To avoid this, the 6-PF-2-K and Fru-2,6-P_2ase activities of the enzyme are intrinsically unequally balanced and modulated by the concentrations of various metabolites (i.e. nucleotide phosphates, F6P, phosphoenolpyruvate, citrate, Fru-2,6-P_2, phosphoglycerate, P_i and 6-phosphogluconate) [2,13]. For example, at physiological concentrations of F6P (30–40μM), the Fru-2,6-P_2ase activity of the testis isozyme should be inhibited (K_i^{F6P} is ~1μM). The activities of the liver and heart isozymes are dramatically regulated by phosphorylation of their N- and C-terminal regulatory domains, respectively [14,15]. The testis and muscle isozymes are not phosphorylated by any protein kinases *in vivo*.

The N-terminal extensions of the liver and testis isozymes are similar, with the major difference being a mutation in the testis enzyme which destroys the recognition sequence for the cAMP-dependent protein kinase (PKA). N-terminal deletion mutations of the testis isozyme suggest that this region modulates the 6-PF-2-K and Fru-2,6-P_2ase activities, and stabilizes the dimer form of the enzyme [11]. Removal of the first 24 or 30 N-terminal amino acids of the testis enzyme causes a protein concentration dependent dissociation of dimers to monomers, and a decrease in thermal stability and resistance to urea denaturation. These same enzymes lose 70% of their 6-PF-2-K activity, while their Fru-2,6-P_2ase activity increases twofold. These kinetic shifts are reminiscent of the effect of phosphorylation of the liver enzyme N-terminal regulatory domain. This suggests that phosphorylation of the liver enzyme may destabilize an interaction of the N terminus with the remainder of the protein.

The 6-PF-2-K/Fru-2,6-P_2ase presented in this structural study is a mutant of the rat testis isozyme [9]. This mutant is one in a series of mutants in which the four tryptophan residues in the isozyme were systematically mutated to phenylalanine as part of a spectroscopic analysis study [16]. Serendipitously, when all of the tryptophans were replaced, the yield of protein from the *Escherichia coli* expression system was dramatically increased, allowing for the adequate production of protein for crystallization trials. We report here the structure of this mutant rat testis 6-PF-2-K/Fru-2,6-P_2ase refined to 2.0 Å resolution. The relations of this structure to both its function and its evolution are discussed.

Results and discussion

Structure determination

Crystals of mutant rat testis 6-PF-2-K/Fru-2,6-P_2ase which diffract to high resolution (≥2.0 Å) were found in the space group $P3_121$ [17]. High resolution X-ray diffraction data were collected for both native and heavy atom derivatized forms of the crystal as summarized in Table 1. A typical course of multiple isomorphous replacement (MIR), solvent flattening, model building, and refinement were used in the structure solution (see Materials and methods for details). The functional form of the protein is a homodimer of 55k Da monomers. One monomer of the protein is found in the crystallographic asymmetric unit, with the dimer twofold rotation coincident with the crystallographic twofold axis. The model has excellent geometry and fits well in continuous electron density, with an overall real space fit statistic of 0.93 for amino acids 37–468 (the C terminus). A portion of the $2F_o–F_c$ electron-density map is shown in Figure 2. The N-terminal 36 amino acids are not visible in the electron density. We confirmed that the N terminus was intact in the crystals by amino acid sequencing protein from the crystal that was the source of the native data used for structure refinement (Native 5). A summary of analyses of the overall quality of the model are presented in Table 2. Only one residue (Lys83) has Φ and ψ angles which are not within the allowed region of a Ramachandran plot; this is explained by the location of this residue near a switch point in the structure which is apparently under strain from crystal contacts.

Monomer structure

The 6-PF-2-K/Fru-2,6-P_2ase monomer is clearly divided into two functional domains as shown in Figures 3a–c. The location of mutations which affect 6-PF-2-K activity [18–21], and the localization of ATPγS in the structure, identify the N-terminal domain as the 6-PF-2-K domain.

Table 1

Data collection and MIR phasing statistics.

	Native 1	Native 5	Thimerosal	Me_3PbOAc	K_2PtCl_4
Data collection					
Resolution (Å)	30–2.2	20–2.0	20–2.7	25–2.3	25–2.8
Completeness*	98 (92)	90 (60)	95 (74)	88 (61)	86 (59)
Multiplicity	5.5	6.8	3.4	5.0	2.9
$I/\sigma(I)$*	11.5 (3.7)	21.6 (2.7)	13.1 (1.9)	13.3 (5.1)	10.1 (1.5)
R_{sym}†	7.1	3.2	5.7	5.3	7.5
Wilson B	22.5	23.6	39.7	27.3	46.4
R_{iso}‡			25.0	24.8	23.9
MIR phasing (20–3.5 Å)					
Soak (mM/h)			10/1.5	10/60	10/3
No. of sites			4	1	1
Total occupancy			2.9	0.9	0.8
Phasing power§			1.2	1.0	0.45
R_{cullis}#			0.81	0.83	0.93

*$I > \sigma(I)$, the number in parentheses is the value in the high resolution shell. †$R_{sym}=\Sigma_h(\Sigma_j|I_{j,h}-<I_h>|/\Sigma I_{j,h})$, where h = set of Miller indices and j = set of observations of reflection h. ‡$R_{iso}=\Sigma_h||F_{Der}|-|F_{Nat}||/\Sigma_h|F_{Nat}|$, where $|F_{Der}|$ = observed derivative structure factor amplitude and $|F_{Nat}|$ = observed native structure factor amplitude. §Root mean square (rms) f_h/residual = $\sqrt{(\Sigma f_h^2/\Sigma(F_{Der}-F_{PH})^2)}$, where f_h = calculated heavy-atom structure factor, F_{PH} = calculated derivative structure factor. #$R_{cullis}=\Sigma||f_h|-(|F_{Der}|-|F_{Nat}|)|/\Sigma||F_{Der}|-|F_{Nat}||$.

Sequence and structural homology with yeast phosphoglycerate mutase [22] and rat acid phosphatase [23] (Fig. 3d), together with the location of mutations which affect Fru-2,6-P_2ase activity [24–28] suggested the C-terminal domain to contain the Fru-2,6-P_2ase activity. In further support of this hypothesis, and most convincingly, the expression of the C-terminal half of the protein in *E. coli* demonstrated full Fru-2,6-P_2ase activity [6], the C-terminal domain is therefore clearly the Fru-2,6-P_2ase domain. The

Figure 2

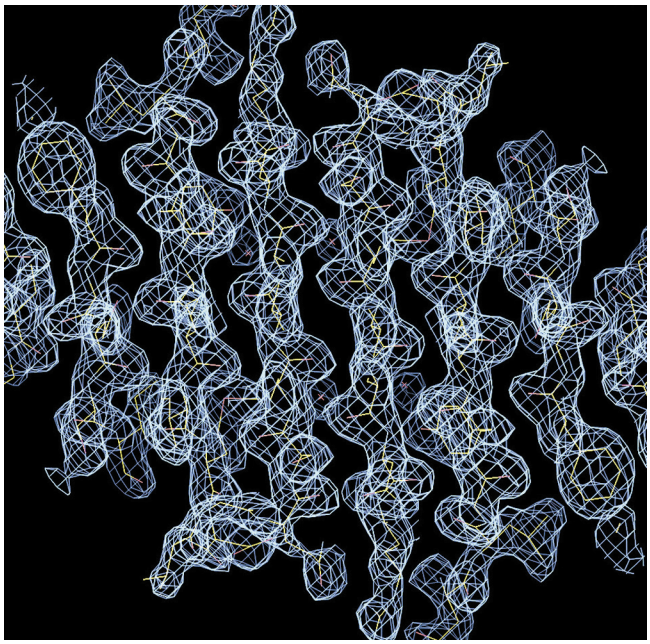

The final $2F_o-F_c$ electron-density map including data from 20–2.0 Å, contoured at 1σ above the mean for the entire map. The region shown is the center of the β sheet which traverses the 6-PF-2-K dimer through the twofold crystallographic axis.

Table 2

Final model statistics.

Data		
Resolution (Å)	6–2.0	20–2.0
R_{work} (%)	18.3	20.6
R_{free} (%)	25.0	27.2
No. of reflections ($F \geq \sigma(F)$)	29 479	30 655
Model		
No. of amino acids	432/468*	
No. of protein atoms	3 534	
No. of heteroatoms	47	
No. of water molecules	319	
No. of refinement parameters	3 900	
Observations/parameter	1.89	
Coordinate error (Å)		
Luzzati	0.29	
SIGMAA	0.29	
Stereochemistry		
Rms deviation		
bond lengths (Å)	0.01	
bond angles (°)	1.55	
improper angles (°)	1.43	
Thermal parameters		
Mean B factor		
main chain	29.0	
side chain	33.5	
protein/hetero	31.8	
solvent	44.2	
Overall B factor (Wilson plot)	23.6	

*Of the 468 expected amino acids 432 were modeled, the N-terminal 36 amino acids were not included in the structure.

Figure 3

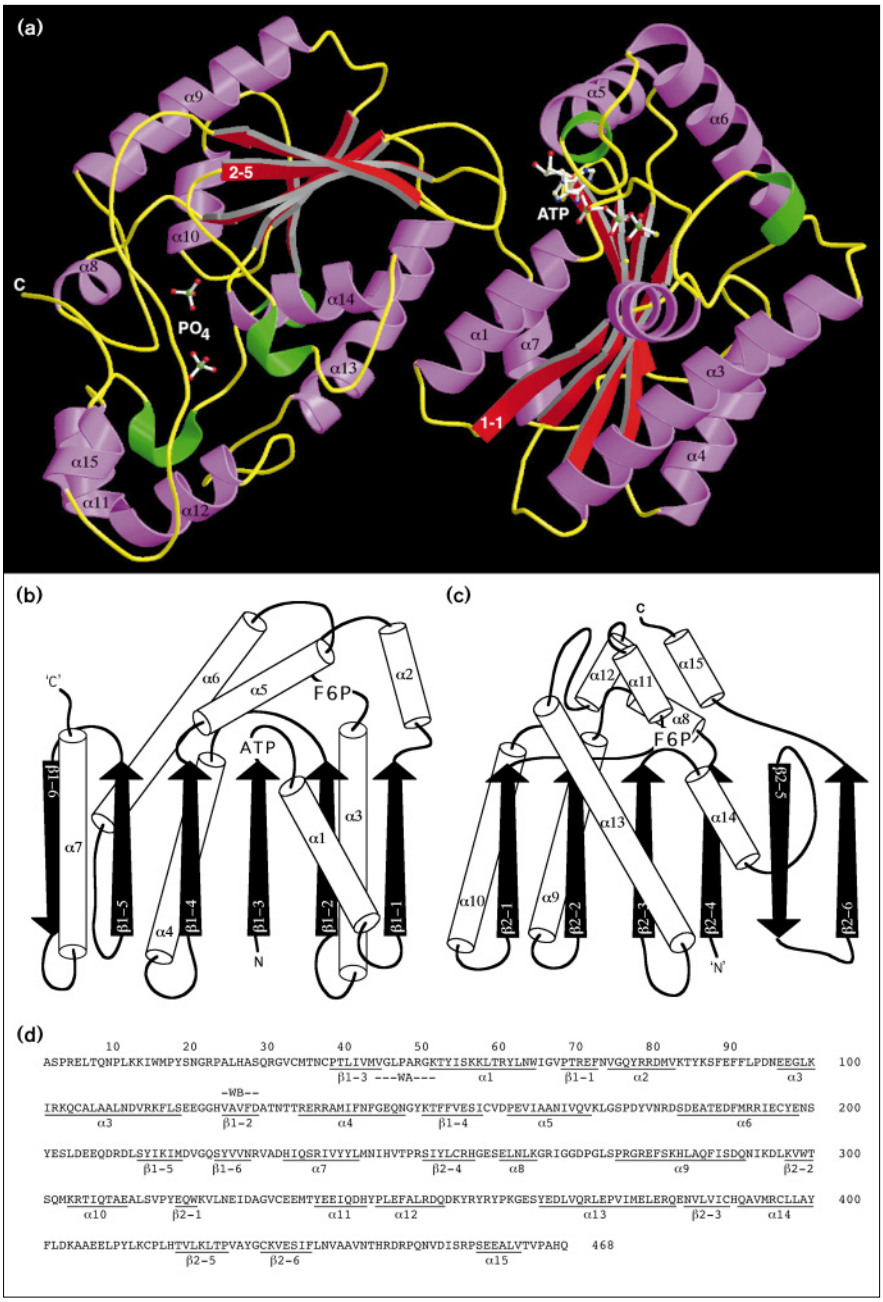

6-PF-2-K/Fru-2,6-P_2ase monomer structure. (a) Ribbon diagram of the 6-PF-2-K/Fru-2,6-P_2ase monomer with the 6-PF-2-K domain to the right and the Fru-2,6-P_2ase domain on the left. α Helices are colored purple and labeled α1–α15, β strands are in red, with one strand of each sheet labeled. 3_{10} Helices are colored green, and random coil is in yellow. Ball-and-stick models of the bound ATP in the 6-PF-2-K domain, and the two bound phosphates in the Fru-2,6-P_2ase domain are also included. The helical subdomain of the Fru-2,6-P_2ase domain is at the lower left of this view. (b,c) Topology diagrams for the 6-PF-2-K and Fru-2,6-P_2ase domains; α helices are represented as cylinders, β strands as arrows. The two β sheets are termed β1 and β2, the individual β strands are numbered sequentially 1–6. The locations of the ATP- and F6P-binding sites are indicated. The lengths of the secondary structure elements and the loops which connect them are not drawn to scale. (d) Sequence of the rat testis 6-PF-2-K/Fru-2,6-P_2ase protein. Locations of secondary structure elements are underlined and labeled. The locations of the Walker A (WA) and Walker B (WB) motifs are also indicated [29]. The 6-PF-2-K domain extends from position 1–250, the Fru-2,6-P_2ase domain extends from position 251–468.

6-PF-2-K domain consists of a central six-stranded β sheet, with five parallel strands and an antiparallel edge strand, surrounded by seven α helices (Fig. 3a,b). A Walker A motif, or nucleotide-binding fold (nbf) [29,30] is located at the C-terminal end of the first β strand (β1–3), with the phosphates of a molecule of ATPγS bound in the anion hole of the so-called phosphate-binding loop. The Fru-2,6-P_2ase domain is also a mixed α/β structure, with a six-stranded central β sheet, plus an additional α-helical subdomain that covers the presumed active site of the molecule. In this structure the active site is occupied by two phosphates (lower left in Fig. 3a).

Dimer interactions

The functional form of the enzyme is a dimer, with a single monomer in the crystallographic asymmetric unit. As shown in Figure 4, the monomers associate in a head-to-head fashion with the 6-PF-2-K domains making intimate contact, while the Fru-2,6-P_2ase domains are essentially independent. The 6-PF-2-K β sheet actually continues

Figure 4

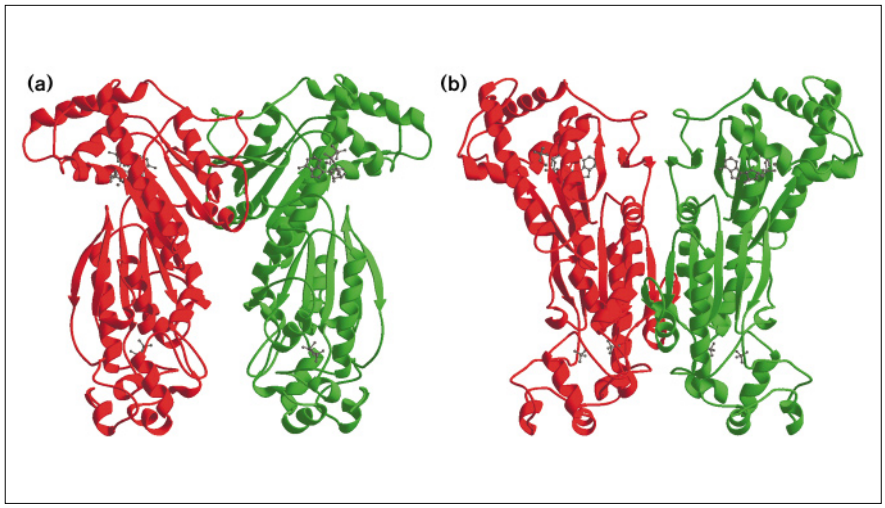

Arrangement of the functional dimer about the crystallographic twofold axis of rotation. The protein monomers are colored red and green, and the ATPγS and PO_4 ligands are in black. (a) The rotation axis is vertical as shown here, with a 180° rotation relating the red and green monomers, it is clear that the Fru-2,6-P_2ase domains (the lower domains) are independent of one another. Only a single salt bridge interconnects the two domains. (b) This image is obtained by rotating the dimer by ~15° about a vertical axis. It is clear that the 6-PF-2-K domains (the upper domains) are quite intimately associated. A β-sheet interaction persists across the dimer interface, generating a 12-stranded β sheet through the dimer. This β-sheet interaction at the dimer interface can be seen just above and between the two ATPγS molecules as seen in this picture.

across the twofold axis via an antiparallel β-strand interaction (Figs 2,4). This interaction extends the 6-PF-2-K central β sheet to form a continuous twelve-stranded intermonomer β sheet. In addition to this interaction at the twofold axis, the α7 helices of the two monomers are in contact, with several interdigitated side chains. Calculated differences in solvent accessible surface area in the monomer and dimer forms of the enzyme, demonstrated 1867 Å^2 of surface area to be buried in the dimer interface, distributed as shown in Table 3. Two thirds of the buried area is located in the 6-PF-2-K/6-PF-2-K interface, implying that the enzyme evolved as a 6-PF-2-K homodimer, with the largely independent Fru-2,6-P_2ase domains tethered to this 6-PF-2-K dimer.

Phosphorylation of an N-terminal subdomain regulates both the 6-PF-2-K and Fru-2,6-P_2ase activities of the liver isozyme, while phosphorylation of the C-terminal subdomain of the heart isozyme regulates only the 6-PF-2-K activity [14,15]. Truncation mutants at the N terminus of the testis and liver isozymes also affect both the 6-PF-2-K and Fru-2,6-P_2ase activities [11,31]. These observations have led to the proposal that the N and C termini are in contact across the dimer interface (i.e. a head-to-tail dimer arrangement) and thus both are positioned to achieve the observed regulation [32,33]. The head-to-head arrangement observed in the testis 6-PF-2-K/Fru-2,6-P_2ase dimer, does not support this explanation of these observations. Furthermore, the high degree of amino acid identity among the 6-PF-2-K/Fru-2,6-P_2ase isozymes virtually rules out the possibility that the other isozymes form a different sort of dimer arrangement than that observed in the testis isozyme.

Table 3

Buried surface area in the dimer interface (monomers A and B).

	6-PF-2-K (A)	Fru-2,6-P_2ase (A)
6-PF-2-K (B)	1253	212
Fru-2,6-P_2ase (B)	212	190

All values given in Å^2.

The absence of the N-terminal subdomain from the model of the testis enzyme does not offer any direct evidence for how this subdomain regulates both the 6-PF-2-K and Fru-2,6-P_2ase activities. However, the location of the first amino acid in the structure (Cys37), the length of the missing segment (36 residues for the testis form, 39 residues by analogy for the liver isozyme), and the assumption that it will adopt some independent fold, place limits on the number of reasonable predictions of its location. A first prediction would place the N-terminal subdomain above helices α3 and α4 (lower right in Fig. 3a), where it would be close to the proposed F6P-binding site and could cause the observed changes in K_m^{F6P}. However, this model would not explain the positive effect of phosphorylation on Fru-2,6-P_2ase activity, as this location is at a distance from the Fru-2,6-P_2ase active sites (as evident in Fig. 4). A second hypothesis would place the N-terminal subdomain in the hinge region between the 6-PF-2-K and Fru-2,6-P_2ase domains. This could be achieved either as an intramonomer or intermonomer interaction. Such an interaction would afford close contact with both domains, and an obvious connection to 6-PF-2-K activity by proximity to the ATP-binding site (Fig. 3a). This is also the location of an interesting interaction between the 6-PF-2-K and Fru-2,6-P_2ase domains, in which the loop between β2–5 and β2–6 (in the Fru-2,6-P_2ase domain) comes quite close to the ATP-binding site of the 6-PF-2-K domain (Fig. 3a).

An intermonomer interaction would explain the loss of dimer stability in the mutant enzymes with N-terminal truncations [11].

Regulation of the heart isozyme by phosphorylation of its C-terminal subdomain is more of a mystery in light of this structure. The heart isozyme has a significant (61 amino acid) addition to its C terminus. In addition, in the testis isozyme, the sites of phosphorylation by PKA and protein kinase C (PKC) are located either within (in the case of PKA) or quite near (in the case of PKC) the C terminus. If the structure of the two isozymes were the same up to the point of the heart isozyme C-terminal extension, the PKA phosphorylation site would be coincident with the Pro465 residue in this structure. In fact, Pro465 is close to the probable binding site for the 6-phosphate of Fru-2,6-P_2 (~9 Å from PO_4 520, see below). This location does not fit well with the experimental evidence however, as phosphorylation of the heart isozyme by PKA affects 6-PF-2-K activity, with no effect on Fru-2,6-P_2ase activity. However, the sequence homology of the heart isozyme begins to break down at position 451 of the testis isozyme, extending the potential size of the divergent C-terminal structure. Thus it seems likely that the C terminus of the heart isozyme has a conformation and location that diverge from the testis enzyme at or near position 451, and no reasonable prediction of where this C-terminal subdomain might be located can be made.

The Fru-2,6-P_2ase domain, and the phosphoglycerate mutase family

As indicated above there is significant structural homology between the Fru-2,6-P_2ase domain and two families of enzymes, the cofactor dependent phosphoglycerate mutases [34], and the acid phosphatases [35]. The fold of all three enzymes includes a central β sheet surrounded by α helices (Fig. 3c), with an additional α-helical subdomain (consisting of two noncontiguous stretches of the protein Glu325–Glu363 and Thr443–Gln468, in the Fru-2,6-P_2ase domain). This subdomain acts as a lid over the active site, and contributes side chains which are involved in substrate binding. An optimized superposition (see Material and methods) of the Fru-2,6-P_2ase domain with the structure of the yeast phosphoglycerate mutase [22] yields a Cα root mean square (rms) deviation for 151 core positions of 1.9 Å, and for the rat prostatic acid phosphatase [23], 110 core positions superimpose with an rms of deviation of 2.0 Å.

These enzymes share a common catalytic mechanism involving a covalent phosphohistidine intermediate [36–38] located in a conserved sequence motif (Z-X-Arg-His-Gly-Glu/Gln-X-X-X-Asn, where Z is a hydrophobic residue, residues 255–262 in the Fru-2,6-P_2ase domain). These conserved amino acids are part of a larger conserved structural motif which includes Arg305, Glu325, and His390, together these residues define the catalytic center of all three enzymes. Figures 5a–d show a diagram of the Fru-2,6-P_2ase reaction as proposed by Pilkis and coworkers [27] while Figure 5e shows the catalytic center of the Fru-2,6-P_2ase domain. In the proposed Fru-2,6-P_2ase reaction, the catalytic histidine (His256) acts by nucleophilic attack on the 2-phosphate of Fru-2,6-P_2. The side chains which are conserved among the enzymes (Arg255, Asn262 and Arg305) are proposed to orient Fru-2,6-P_2 and stabilize the transition state. The second histidine (His390) is proposed to be protonated, with the positive charge stabilizing the transient negative charge on the leaving group oxygen of the transition state. The same histidine is also thought to act as a general acid, protonating the leaving group. A water or hydroxide then attacks the phosphoenzyme intermediate, regenerating the enzyme and producing Pi. For the acid phosphatases, the resolution of the phosphoenzyme intermediate is also hydrolytic, while in the phosphoglycerate mutases, phosphoglycerate acts as the nucleophile which regenerates the enzyme, producing 2,3-diphosphoglycerate.

As shown in Figure 5e, two well ordered phosphates are bound in the active site of the Fru-2,6-P_2ase domain, one bound to the catalytic histidine (PO_4 510, the lower PO_4 in Fig. 5e), the other (PO_4 520) is bound by side chains emanating from the α-helical subdomain, occupying the probable binding site for the 6-phosphate of Fru-2,6-P_2. The spacing between these two phosphates is consistent with several orientations of Fru-2,6-P_2 modeled between them. Despite kinetic evidence that F6P binds in the Fru-2,6-P_2ase active site, and the presence of F6P in the crystallization, there is no electron density which can be clearly interpreted as F6P in the Fru-2,6-P_2ase active site of this crystal structure. Mutagenesis studies in the liver isozyme [26–28] have confirmed the importance to catalysis of several residues neighboring PO_4 510, including the catalytic His256, and Arg255, Arg305, Glu325 and His390 (numbered 258, 257, 307, 327 and 392 in the liver isozyme). In general, the interpretations of the mutagenesis results are consistent with the structure, that is, that the basic residues probably play a role in recruiting/binding the substrate as well as stabilizing the transition state. Close examination of the relationship of His256 and PO_4 510 shows that the histidine Nε is directly in line with a P–O bond. This observation is consistent with the proposed catalytic mechanism involving an inversion of the phosphate geometry on formation of the phosphohistidine intermediate (see Fig. 5e). One conclusion is not supported by the structure, however. Lin *et al.* [27] have proposed that Glu325 acts to maintain His390 in a protonated state. However, in the structure presented in Figure 5e Glu325 is not close enough to His390 to support this conclusion. Instead, Glu325 is acting to 'cap' the helix α14, and could only interact with His390 if a structural rearrangement occurs on substrate binding. The role that the conserved asparagine (Asn262) might play in catalysis has not been addressed

Figure 5

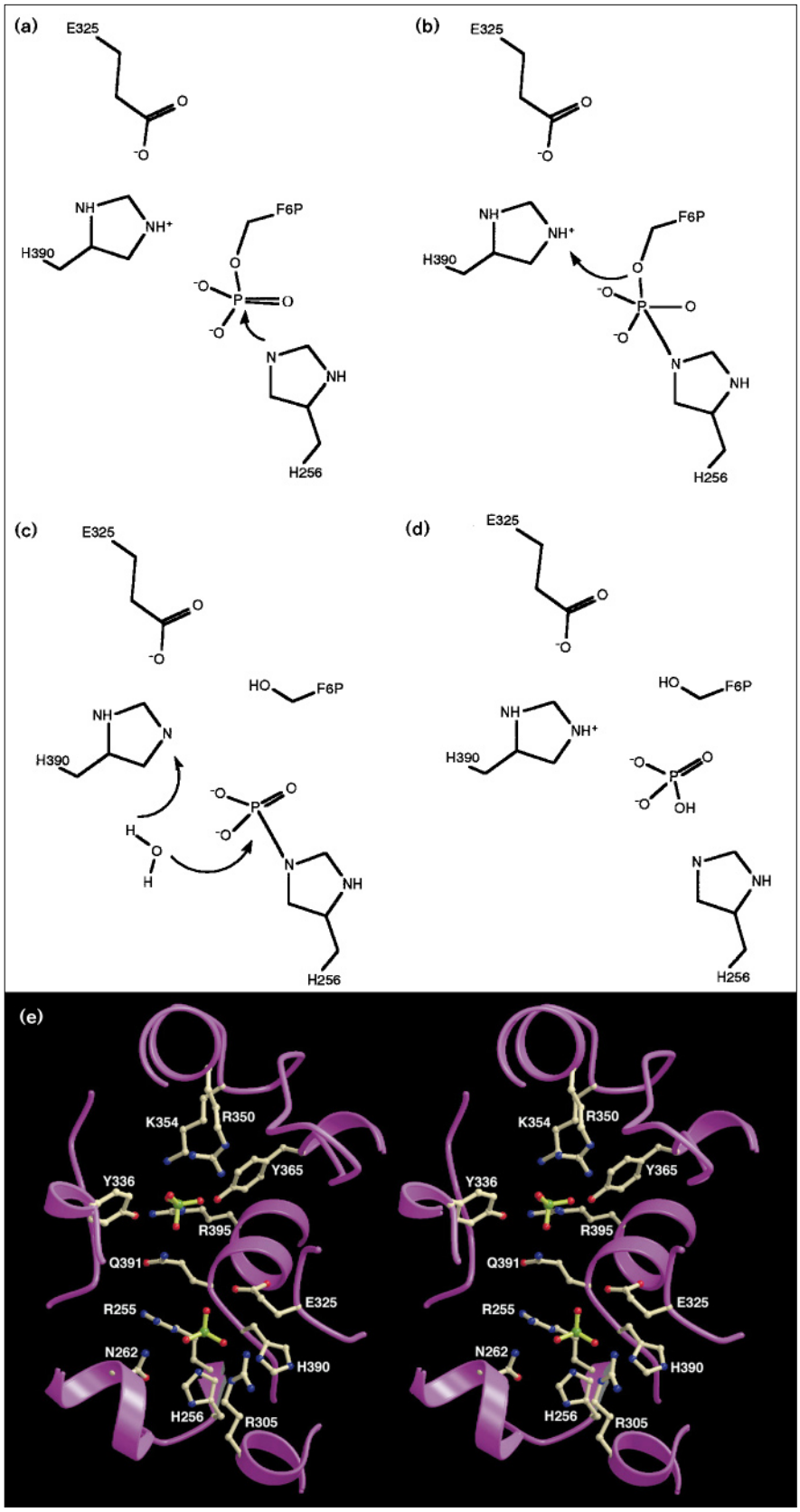

Schematic representation of the Fru-2,6-P_2ase reaction as proposed by Pilkis and co-workers [27]. (**a**) The catalytic histidine (His256) attacks the 2-phosphate of Fru-2,6-P_2. (**b**) The pentacoordinated transition state is shown, stabilized by several salt bridges and/or hydrogen bonds from side chains which are not shown (Arg255, Arg305 and Asn262). His390 is proposed to be maintained in a protonated state by Glu325, and this proton will be used in the resolution of the transition state in favor of production of the protonated F6P product. (**c**) The phosphohistidine intermediate is shown, with a water molecule in proximity. This water will attack the phosphohistidine, generating P_i and newly protonated His390 as shown in (**d**). (**e**) Stereo view of the Fru-2,6-P_2ase active site. Phosphates are shown in ball-and-stick representation with phosphorous atoms in green, oxygens in red, and bonds in gray. The lower phosphate as viewed here is bound in the catalytic active site, adjacent to His256 which is the residue which forms the phosphohistidine intermediate. The upper phosphate is bound in the pocket which is specific for the 6-phosphate of Fru-2,6-P_2, surrounded by several positively charged residues (Lys354, Arg350 and Arg395). Side chains which interact with the phosphates are shown in ball-and-stick representation, with oxygen atoms in red, nitrogen atoms in blue, and carbon atoms and bonds in gray.

experimentally, but its proximity to PO_4 510 would suggest that it may also play a role in substrate recruitment or transition state stabilization. These issues await confirmation by substrate analogue bound or product/transition state mimic bound structures.

The binding site of PO_4 520 (the upper PO_4 in Fig. 5e) has also been studied by mutagenesis of the liver isozyme [24,25], and was implicated as the binding site for the 6-phosphate of Fru-2,6-P_2 by mutations of Arg352, and Lys356 (Arg350, Lys354 in the testis isozyme and Fig. 5e). Other residues which are in contact with this phosphate are Gln391, Tyr336, Tyr365 and Arg395, although their role in substrate binding has not been tested experimentally. One mutation which alters Fru-2,6-P_2 binding (Arg360 in the liver isozyme [24]) cannot be explained by the structure, as the analogous Arg356 in the testis isozyme is a solvent exposed residue, and not close to the Fru-2,6-P_2-binding site.

The crystal structure of a truncated rat liver Fru-2,6-P_2ase domain (amino acids 252–440 of the rat liver bifunctional enzyme, analogous to 250–438 in the testis isozyme) was recently reported [39]. The truncated liver Fru-2,6-P_2ase domain is in general quite similar to the testis Fru-2,6-P_2ase domain reported here, including a phosphate bound in the active site, with analogous residues involved in phosphate coordination. No second phosphate was observed in the presumed 6-phosphate-binding site of the liver isozyme, but docking studies came to similar conclusions (as described above) for the location and binding of the phosphate as observed in the testis isozyme structure reported here.

The most significant difference is the 30 amino acids missing from the C terminus of the truncated liver Fru-2,6-P_2ase domain. This truncation has led to at least two significant differences between the structures. Firstly, the absence of the C terminus has led to a much more open active site than is seen in the testis isozyme. As described by Lee *et al.* [39], the truncated liver domain has a funnel-shaped active site, with the large end of the funnel between two loops (260–273 and 328–357 in the liver enzyme). The presence of the C terminus in a position analogous to that seen for the testis isozyme would significantly occlude this opening. The second apparent consequence of the missing peptide is the formation of a dimer of Fru-2,6-P_2ase domains with C2 point group symmetry, the asymmetric unit of the liver Fru-2,6-P_2ase crystal. This dimer interface coincides with the location of the C terminus of the testis isozyme, and its presence in the liver isozyme would preclude the formation of this dimer. Furthermore, in contrast to the extended β-sheet interaction at the dimer interface of the testis 6-PF-2-K domains described above, the truncated liver Fru-2,6-P_2ase domain interface involves mainly side-chain interactions. We would thus argue that the dimer observed in the intact testis isozyme is the natural dimer, while that observed for the liver Fru-2,6-P_2ase domain is a consequence of the truncation of the C terminus.

The 6-PF-2-K domain, NMP kinases and G proteins

The binding of ATP by the 6-PF-2-K domain is very much like that seen in other proteins which possess a Walker A nbf (i.e. Gly-X-X-Gly-X-Gly-Lys-Thr, amino acids 45–52 in the 6-PF-2-K domain). Table 4 summarizes the nucleotide–protein interactions which are also displayed in Figure 6a. The N terminus of the α1 helix and the main chain nitrogen atoms of residues 48–53 form an anion hole that acts as a phosphate-binding pocket. In addition, the conserved lysine residue of the nbf (Lys51) interacts with both the β- and γ-phosphates of ATP, in a position which is consistent with the proposal that it remains bound to the γ-phosphate during phosphoryl transfer [30]. The conserved threonine of the nbf (Thr52), and the conserved aspartate (Asp128) of the Walker B motif (Z-Z-Z-Z-Asp, where Z is any hydrophobic residue) provide two ligands for the octahedral Mg^{2+} ion (MG 501) coordination; the β- and γ-phosphates of ATP provide another two ligands. The remaining two Mg^{2+} coordination positions are not occupied.

The binding pocket for the nucleotide forms very few specific interactions with the polar groups of the adenine moiety. The interactions mainly involve stacking between the adenine rings and nonpolar side chains (Cys158, Val163, Val220 and Val246). A single hydrogen bond is formed between the Oδ oxygen of Asn167 and the adenine N6. The substitution of a carbonyl at this position in a guanine ring would still allow for this hydrogen bond after a simple

Table 4

ATP–protein interactions.

ATPγS atoms	6-PF-2-K/Fru-2,6-P_2ase atoms
Phosphates	
Pγ O1	K172 Nζ, water 1005
O2	K51 Nζ, water 1005
O3	Mg^{2+}501, water 1003
Pβ O1	R49 N, K51 N, K51 Nζ
O2	T52 N, Mg^{2+}501, water 1003, T52 Oγ2
O3	A48 N, K172 Nζ
Pα O1	Y53 N
O2	K172 Nζ, Y427 OH, water 1003
O3	G50 N
Ribose	
O3′	Q170 Nε2, N167 Nδ2
ring plane	Y53, N167
Adenine	
N3	N167 Oδ1
N6	water 664, water 693
ring plane	V220, V246, main chain 49–50

Figure 6

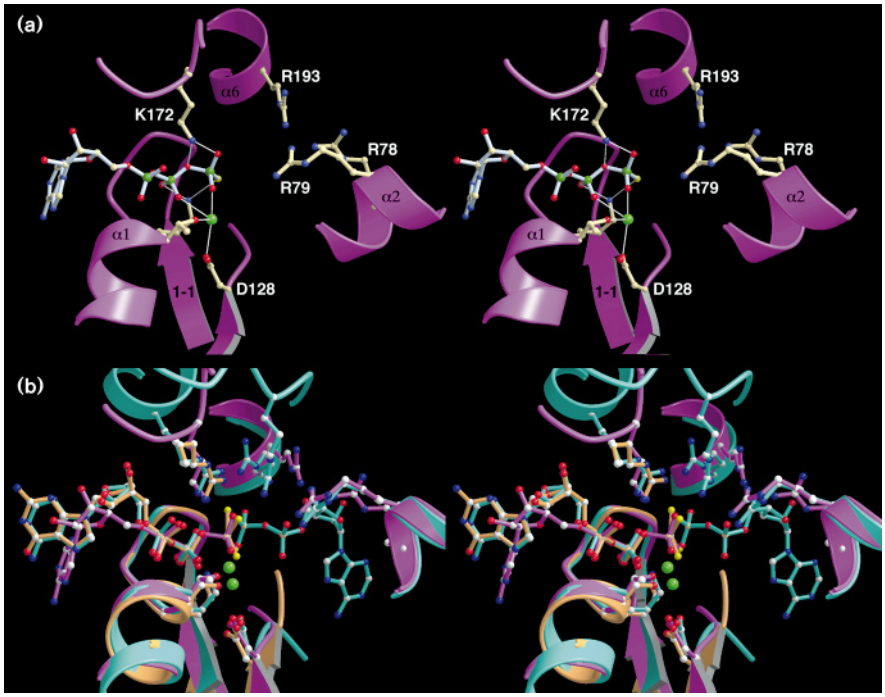

Nucleotide–protein interactions of the 6-PF-2-K domain. (a) Stereo view of ATPγS bound in the 6-PF-2-K active site. Close contacts between the ATPγS, Mg^{2+}, Lys172, Lys51, Thr52, and Asp128 are shown as white lines. Also shown are Arg78, Arg79 and Arg193 residues which have been shown to affect F6P binding. The multiple hydrogen bonds formed between the phosphate oxygens and the main chain nitrogens in the loop connecting β1-1 and α1 are not shown. (b) Stereo view of the superposition of the 6-PF-2-K (purple), the G protein $G_{i\alpha}$(orange), and uridylate kinase (UDK) (turquoise) active sites. The $G_{i\alpha}$ coordinates are from the $AlFl_4^-$ transition state analogue structure [44], and thus include the planar $AlFl_4^-$ moiety shown in yellow. The UDK structure includes two bound ADP molecules, thus representing the ADP–product complex [42]. The structures were superimposed using only the protein coordinates of the ATP-binding loops; this results in an excellent superposition of the 6-PF-2-K γ-phosphate, the $G_{i\alpha}$ $AlFl_4^-$, and the UDK product (β-phosphate).

180° exchange of the Asn167 Nδ and Oδ atoms, leading to an Nδ–carbonyl interaction. This information predicts that GTP should substitute freely for ATP as a phosphate donor in the kinase reaction.

It has been speculated that the 6-PF-2-K domain resembles phosphofructokinase (PFK), and that the 6-PF-2-K reaction proceeds with a mechanism similar to that of PFK (i.e. a nucleophile, glutamate or aspartate, activates the sugar hydroxyl group to potentiate its nucleophilic attack on the γ phosphate of ATP) [4,40]. Acting on this assumption, and lacking any structural data, Uyeda and coworkers produced a complete series of Glu/Asp→Ala mutants (Uyeda *et al.*, unpublished data) in the 6-PF-2-K domain. Except for the aspartate residue that coordinates the ATP associated Mg^{2+} ion (Asp128, Fig. 6), no mutant significantly lowered the catalytic rate of the 6-PF-2-K reaction. This result calls into question the exact catalytic mechanism of the 6-PF-2-K reaction. Sequence analysis does not predict any significant relation between the 6-PF-2-K domain and other known proteins. However, examination of the 6-PF-2-K fold reveals that this domain is structurally related to the family of nucleoside monophosphate kinases (NMP kinases) and to the catalytic core of the G proteins. The calculated similarities of Cα positions in their cores were: 1.9 Å (for 102 residues of adenylate kinase [41]); 2.1 Å (for 129 residues of uridylate kinase UDK [42]); 1.5 Å (for 52 residues of p21-Ras [43]); and 1.5 Å (for 48 residues of the G protein, $G_{i\alpha}$ [44]). The catalytic centers are remarkably similar among the structures (shown in Fig. 6b). This striking structural homology suggests there is a potential similarity in their catalytic mechanisms, divergent from a large group of nucleotide triphosphate phosphotransferases in which a nucleophilic activation of the substrate is requisite for catalysis [45,46].

It has been proposed that the NMP kinases and the G proteins catalyze their reactions by stabilization of the transition state, without a nucleophilic activation of the substrate [41,42,44]. The convergent similarity of several catalytic and structural residues from divergent regions of all three structures (NMP kinases, G proteins and 6-PF-2-K) implies that they may share this common catalytic mechanism. One way of thinking about such a mechanism is to consider an analogy with ATP/GTP hydrolysis in solution, in which a transient negative charge must accumulate on the β–γ bridge oxygen during that transition state [47]. Relevant to this mechanism is the superposition of Lys172 of the 6-PF-2-K domain, Arg142 of yeast UDK, and Arg178 of $G_{i\alpha}$, as shown in Figure 6b. These positively charged residues are positioned so as to stabilize a negative charge on the β–γ bridge oxygen, and are not conserved among all nbf containing proteins (i.e. EF-Tu, RecA and ADP ribosylation factor). Furthermore, Arg178 of $G_{i\alpha}$ was shown to be recruited as a nucleotide contact residue only in the $AlFl_4$-transition state mimic complex [44]. This information, in combination with the lack of a nucleophile near the proposed active site described above, and the structural homology with the NMP kinases and G proteins, make it increasingly likely that the 6-PF-2-K reaction mechanism is

Figure 7

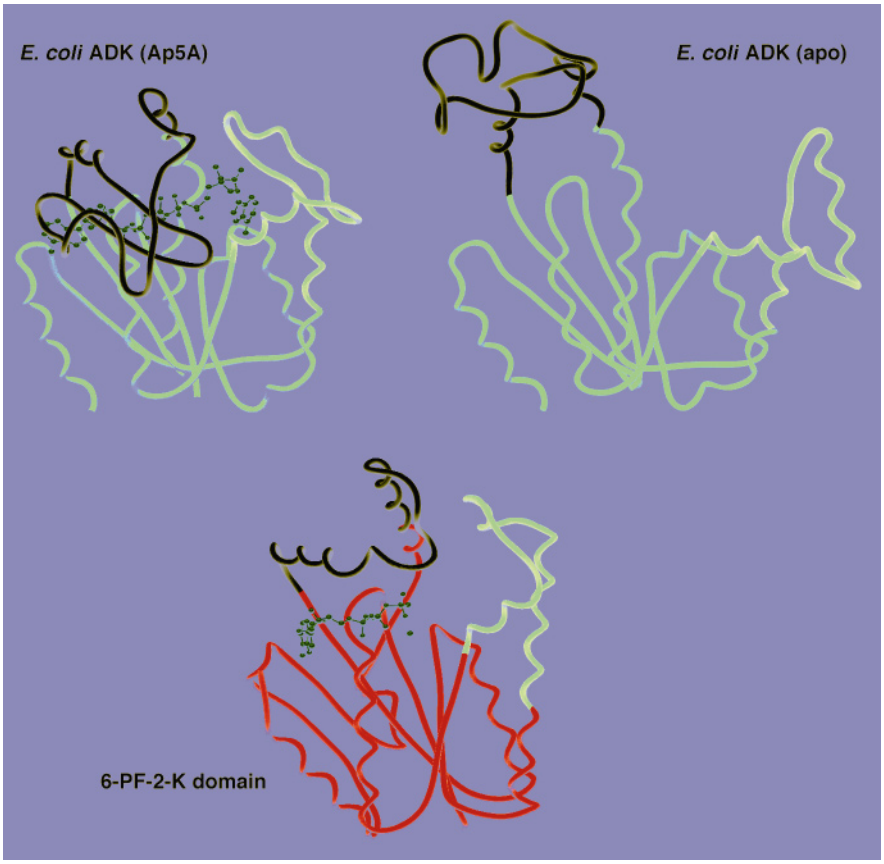

The similarity of *E. coli* adenylate kinase ATP- and AMP-binding loops to the proposed ATP- and F6P-binding loops of the 6-PF-2-K domain. Ribbon diagrams of the 6-PF-2-K domain (purple) and *E. coli* adenylate kinase (ADK) (green) in the substrate-bound (Ap5A) and substrate-free (apo) conformations are shown [41,49]. The mobile loops of ADK involved in ATP and AMP (substrate) binding are colored in white and yellow, respectively. The 6-PF-2-K domain is presented in the same orientation, with the proposed mobile ATP- and F6P-binding loops also colored white and yellow, respectively. In the absence of substrates, the *E. coli* ADK ATP- and AMP-binding loops are in an open conformation. Ap5A is an inhibitor of *E. coli* ADK which mimics both ATP and substrate. In the presence of Ap5A, both binding loops of the enzyme are in a closed conformation. The 6-PF-2-K domain has bound ATP, and the ATP-binding loop is in a closed conformation. Despite the absence of F6P from the structure, the F6P loop appears to be at least partially closed, possibly due to crystal contacts.

distinct from that of PFK. We propose that the 6-PF-2-K domain operates via a transition state stabilization mechanism alone, possibly with greater similarity to a dissociative reaction mechanism than previously assumed. Confirmation of this hypothesis will require further kinetic and structural studies.

Another similarity between the 6-PF-2-K domain and the NMP kinase structures is highlighted in Figure 7. The NMP kinases have two mobile segments responsible for ATP and substrate binding (shown in Fig. 7). These segments were initially identified in a series of adenylate kinase (ADK) structures from different species [48], and

Figure 8

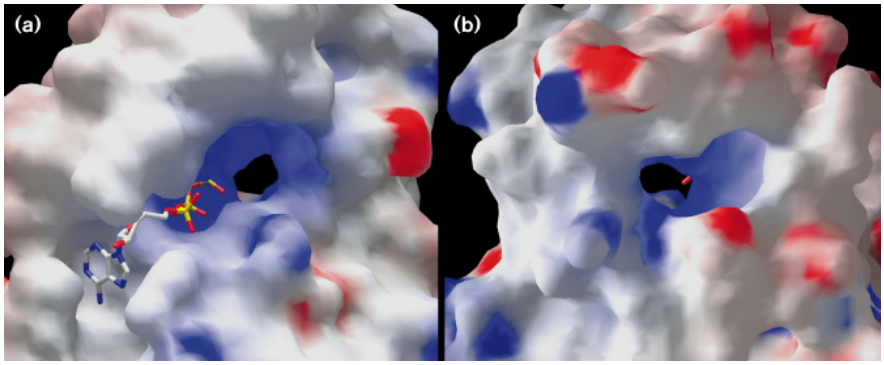

Molecular surface representation of the 6-PF-2-K domain in the vicinity of the catalytic center. (a) The ATP-binding site of the enzyme; in this view the ATP-binding loop is above the ATP. The γ-phosphate is partially obscured by the surface of Lys172. There is a predominant positive potential in the phosphate-binding pocket of the enzyme. Beyond the γ-phosphate, a 'hole' through the enzyme is plainly visible. This hole is coincident with the proposed F6P-binding site, and is formed at the interface between the F6P-binding loop and the remainder of the 6-PF-2-K domain. (b) The 6-PF-2-K domain is rotated in this view to look back towards the ATP γ-phosphate through the 'hole' in the enzyme. The surfaces are color-coded for the electrostatic potential at the surface, with the most blue and red colors representing potentials of +12 and –12 kcal, respectively. The surfaces and potential maps were generated in the absence of ATP. (Figure generated by GRASP [61].)

more recently confirmed in a comparison of ligand-bound and apo-ADK from *E. coli* [49]. The proposed function of these mobile domains in the NMP kinases is to exclude solvent from the vicinity of bound ATP to prevent futile ATP hydrolysis. Analysis of temperature factors in our structure shows that the 6-PF-2-K domain shares this flexibility in analogous regions of its topology (Fig. 7). Thus the segments of the 6-PF-2-K domain including amino acids 74–100 and 159–194 have average Cα B factors of 34 and 36 respectively compared to an average Cα B factor of 26 for the remainder of the domain. By analogy to ADK, these regions are predicted to be mobile segments which trap F6P and ATP, respectively. In the 6-PF-2-K domain the ATP-binding loop is closed, consistent with the fact that the structure contains bound ATP. The F6P-binding loop appears to be in a partially closed conformation despite a lack of F6P in the binding site. In the crystal, the conformations of both the ATP- and F6P- binding loops may be stabilized in their observed positions by crystal packing interactions. The theme of lobed structures with probable induced fit changes on substrate/ATP binding pervades the structures of other kinases as well, including PFK [50], hexokinase [51], phosphoglycerate kinase [52], and pyruvate kinase [53].

While it has not been possible to refine the position of a molecule of F6P in the active site of the 6-PF-2-K domain, there are clear indications as to where the F6P-binding site is located. Firstly, the site-specific mutants which affect the 6-PF-2-K activity via an effect on K_m^{F6P} map to a single region of the structure (Arg102, Arg193 and Arg136) [18–21] (Uyeda *et al.*, unpublished data). Secondly, this region is coincident with the NMP-binding sites of the NMP kinases, and is adjacent to the bound ATPγS. Finally, there is residual electron density in this location, which cannot be modeled as water. Based on these concordant pieces of circumstantial evidence, the binding site for F6P can be predicted with some confidence to be analogous to the NMP-binding sites of the NMP kinases (Fig. 6b). As shown in Figure 8, there is a 'hole' in the structure, at the interface between the body of the 6-PF-2-K domain and the F6P-binding loop, with an appropriately placed positive electrostatic potential to recruit and bind the negatively charged 6-phosphate of F6P.

Biological implications

Glycolysis is essential for energy production from glucose and for the formation of the three carbon compounds used as precursors for the synthesis of amino acids, fatty acids, and cholesterol. The rate of glycolysis in the liver is integral to the maintenance of blood glucose levels. The importance of glucose homeostasis is obviated by the various forms of diabetes where unregulated glucose levels cause life-threatening results. Fructose-2,6-bisphosphate (Fru-2,6-P_2) is the physiological activator of phosphofructokinase (PFK), and hence the cytosolic concentration of Fru-2,6-P_2 regulates glycolysis. In turn, the bifunctional enzyme 6-phosphofructo-2-kinase/fructose-2,6-bisphosphatase (6-PF-2-K/Fru-2,6-P_2ase) controls the levels of Fru-2,6-P_2, and thus the activities of this enzyme are central to the control of glycolysis.

The crystal structure of 6-PF-2-K/Fru-2,6-P_2ase confirms predictions that the kinase and phosphatase activities are found in separate domains. The Fru-2,6-P_2ase domain is a member of the phosphoglycerate mutase family. Contrary to predictions that the 6-PF-2-K domain would resemble PFK (6-PF-1-K), it is related to the nucleotide monophosphate (NMP) kinases, and the catalytic domain of G proteins. The fine structure of the 6-PF-2-K active site and its homology to these other proteins imply that the 6-PF-2-K domain operates by transition state stabilization. This is in contrast to the PFK mechanism, which involves a nucleophilic activation of the Fructose-6-phosphate hydroxyl group. The 6-PF-2-K domain has mobile ATP- and substrate-binding loops analogous to those in the NMP kinases.

This structure will lead to the design of specific experiments to test the mechanisms of catalysis, and the coordinate regulation of catalytic activities. It will also serve as a good model for the catalytic domains of the remaining isozymes, because of the high homology among them. Ultimately, this structure may lead to the design of novel therapeutic compounds to alter the rate of glycolysis in the liver for treatment of type II diabetes, or in the myocardium for intervention in ischemic heart disease.

Materials and methods

Crystallization and heavy atom derivatization

The W0 mutant (all tryptophans mutated to phenylalanine) of the rat testis isozyme of 6-PF-2-K/Fru-2,6-P_2ase was expressed in *E. coli* and purified as described [11,16]. Crystals were prepared by sitting drop vapor diffusion of 10 mgml^{-1} protein (in 50 mM Tris-PO_4 pH 7.5, 5% glycerol, 0.5 mM EDTA, 1% PEG 400, 10 mM DTT, 3 mM $MgCl_2$, 1 mM ATPγS and 1 mM F6P) mixed 50 : 50 with a well solution of 15% PEG 4000, 50 mM succinate pH 6.2, 10 mM HEPES pH 7.0 and 2% n-octyl-glucoside, as previously reported [17]. Heavy-atom derivatives were prepared by equilibrating crystals in a surrogate mother liquor (16% PEG 4000, 50 mM succinate pH 6.2, 10 mM HEPES pH 7.0, 50 mM Tris-PO_4 pH 7.5, 5% glycerol, 0.5 mM EDTA, 1% PEG 400, 10 mM DTT and 3 mM $MgCl_2$) containing heavy atoms as listed in Table 1.

Data collection and processing

Crystals were prepared for flash freezing in liquid ethane by serial transfers into solutions of surrogate mother liquor (see above) with increasing concentrations of glycerol (10–25 % in 5 % steps). Crystals were maintained at 120°K in a dry nitrogen stream using a Molecular Structure Corporation cryodevice. Data were collected on a Xuong-Hamlin multiwire area detector (Native 1, K_2PtCl_4 and Thimerosal derivatives) or on an R-Axis II (Rigaku) image plate detection system (Native 5 and Me_3PbOAc derivative), both systems were mounted on Rigaku rotating-anode generators and operated at 50 mA, 100 kV, with a graphite monochromater, or 20 mA, 100 kV with double mirror focusing (Molecular Structure Corporation), respectively. Xuong-Hamlin data were integrated using the program XDS [54], R-Axis data using the program Denzo [55].

All data were merged and scaled in Scalepack [55] and formatted for subsequent use in either the CCP4 suite [56] or X-PLOR [57].

MIR phasing, model building and refinement

Potential heavy-atom derivative diffraction data were scaled to native data using the Scaleit program in CCP4. Difference Patterson maps and vector verification (RSPS in CCP4) immediately identified a single heavy-atom site in the Me_3PbOAc derivative. MLPHARE (CCP4) was used to refine the position and occupancy of this site, and the resulting SIR phases were then used to search for additional derivatives by difference Fourier analysis in conjunction with Patterson and vector verification procedures. The handedness of the structure was determined, and the three derivatives in Table 1 were refined (using the anomalous dispersion data, in MLPHARE; MIR phases were calculated resulting in a figure of merit of 0.53 for 20–3.5 Å data. The MIR phases were improved by solvent flattening and histogram matching (calculated solvent content 49 %, used 40 % in the program DM in CCP4).

Electron-density maps were calculated with these improved phases with data from 20–3.5 Å, 20–3.0 Å and 20–2.8 Å, with the lowest resolution map being the most interpretable. The 3.5 Å map was skeletonized, and the skeleton used as a guide to build a Cα chain trace in the program O (version 5.1) [58]. The Cα trace was then converted with the Lego_CA command (O) to include 330 alanine residues in seven segments. This partial structure was subjected to positional refinement in X-PLOR, and the resulting partial structure phases were subsequently combined with the MIR phases, using weights computed in SIGMAA [59]. In two further similar rounds of model building, a continuous polypeptide was constructed, and side chain density was clear enough to unambiguously place the amino acid sequence into the observed electron density for amino acids 37–468. This initial model refined well in X-PLOR, extending the resolution in steps from 3.5 Å to 3.0 Å, 2.5 Å and 2.2 Å, refining positions and individual B factors. Simulated annealing at 2.2 Å and subsequent positional refinement yielded an R_{work} of 27.0 % and an R_{free} of 38.6 % for data from 6–2.2 Å with $F \geq 3(\sigma F)$. Several rounds of model correction and refinement and the addition of ADP, Mg, two PO_4 groups and 60 water molecules yielded a model with an R_{work} of 20.9 % and an R_{free} of 29.1 %. At this point a higher resolution native data set was collected, and the refinement proceeded against that data (Native 5, Table 1). Due to persistent density at a covalent distance from the ADP β-phosphate, a γ-phosphate was added, and assigned an arbitrary reduced occupancy (0.4). Despite the presence of 1 mM F6P in the crystallization mixture, no ordered F6P could be modeled in either the 6-PF-2-K or Fru-2,6-P_2ase active sites. There is residual density in both presumed F6P-binding sites, but none of the possible interpretations of this density as F6P were refineable. We assume that the binding sites are partially occupied by several orientations of F6P or some other competitor molecule(s). Some of this residual density was eventually modeled as water, but difference density remains, indicating that some more electron dense species occupy these binding sites. Addition of water molecules and an ordered glycerol and further refinement yielded the final model reported here (Table 2).

Structure comparisons

Structural superpositions were calculated with the lsq_explicit and lsq_improve facilities within O [58]. Parameters for the superposition were set so that only contiguous stretches of three or more residues were included in the superposition. Atom pairs with an rms deviation greater than 3.8 Å were excluded from the calculations.

Accession number

Coordinates are being deposited with the Protein Data Bank [60].

Acknowledgements

We would like to thank Cu Nguyen for excellent technical assistance in the preparation and crystallization of the enzyme, and Ravichandran Kurumbail, whose enthusiasm for this project kept it alive in the early stages. This work was supported by The Welch Foundation (CH), Howard Hughes Medical Institute (JD), the Veterans Administration (KU), and the NIH (DK16194, KU).

References

1. Pilkis, S.J., Claus, T.H., Kurland, I.J. & Lange, A.J. (1995). 6-Phosphofructo-2-kinase/fructose-2,6-bisphosphatase: a metabolic signaling enzyme. *Annu. Rev. Biochem.* **64**, 799–835.
2. Rousseau, G.G. & Hue, L. (1993). Mammalian 6-phosphofructo-2-kinase/fructose-2,6-bisphosphatase: a bifunctional enzyme that controls glycolysis. *Prog. Nucl. Acid Res. Mol. Biol.* **45**, 99–127.
3. Uyeda, K. (1991). Phosphofructokinase and fructose-6-phosphate, 2-kinase: fructose-2,6-bisphosphatase. In *Study of Enzymes II.* (Kuby, S.A., ed), pp. 445–456, CRC Press, Boca Raton, FL.
4. Bazan, J.F., Fletterick, R.J. & Pilkis, S.J. (1989). Evolution of a bifunctional enzyme: 6-phosphofructo-2-kinase/fructose-2,6-bisphosphatase. *Proc. Natl. Acad. Sci. USA* **86**, 9642–9646.
5. Algaier, J. & Uyeda, K. (1988). Molecular cloning, sequence analysis, and expression of a human liver cDNA coding for fructose-6-P,2-kinase:fructose-2,6-bisphosphatase. *Biochem. Biophys. Res. Commun.* **153**, 328–333.
6. Lee, Y.H., Okar, D., Lin, K. & Pilkis, S.J. (1994). Mechanism of modulation of rat liver fructose-2,6-bisphosphatase by nucleotide triphosphates. *J. Biol. Chem.* **269**, 11002–11010.
7. Darville, M.I., Crepin, K.M., Hue, L. & Rousseau, G.G. (1989). 5′ Flanking sequence and structure of a gene encoding rat 6-phosphofructo-2-kinase/fructose-2,6-bisphosphatase. *Proc. Natl. Acad. Sci. USA* **86**, 6543–6547.
8. Tsuchiya, Y. & Uyeda, K. (1994). Bovine heart fructose-6-phosphate, 2-kinase: fructose-2,6-bisphosphatase mRNA and gene structure. *Arch. Biochem. Biophys.* **310**, 467–474.
9. Sakata, J., Abe, Y. & Uyeda, K. (1991). Molecular cloning of the DNA, expression and characterization of rat testis fructose-6-phosphate, 2-kinase:fructose-2,6-bisphosphatase. *J. Biol. Chem.* **266**, 15764–15770.
10. Ventura, F., Rosa, J.L., Ambrosio, S., Pilkis, S.J. & Bartrons, R. (1992). Bovine brain 6-phosphofructo-2-kinase/fructose-2,6-bisphosphatase. Evidence for a neural-specific isozyme. *J. Biol. Chem.* **267**, 17939–17943.
11. Tominaga, N., Minami, Y., Sakakibara, R. & Uyeda, K. (1993). Significance of the amino terminus of rat testis fructose-6-phosphate, 2-kinase:fructose-2,6-bisphosphatase. *J. Biol. Chem.* **268**, 15951–15957.
12. Kitamura, M. & Uyeda, K. (1988). Purification and characterization of myocardial fructose-6-phosphate, 2-kinase and fructose-2,6-bisphosphatase. *J. Biol. Chem.* **263**, 9027–9033.
13. Sakurai, T., Johnson, J.H. & Uyeda, K. (1996). Islet fructose 6-phosphate, 2-kinase:fructose 2,6-bisphosphatase: isozymic form, expression, and characterization. *Biochem. Biophys. Res. Commun.* **218**, 159–163.
14. Kurland, I.J., El-Maghrabi, M.R., Correia, J.J. & Pilkis, S.J. (1992). Rat liver 6-phosphofructo-2-kinase/fructose-2,6-bisphosphatase. Properties of phospho- and dephospho- forms and of two mutants in which Ser32 has been changed by site-directed mutagenesis. *J. Biol. Chem.* **267**, 4416–4423.
15. Kitamura, M., Kangawa, K., Matsuo, H. & Uyeda, K. (1988). Phosphorylation of myocardial fructose-6-phosphate, 2-kinase: fructose-2,6-bisphosphatase by cAMP-dependant protein kinase and protein kinase C. Activation by phosphorylation and amino acid sequences of the phosphorylation sites. *J. Biol. Chem.* **263**, 16796–16801.
16. Watanabe, F., Jameson, D.M. & Uyeda, K. (1996). Enzymatic and fluorescence studies of four single tryptophan mutants of rat testis fructose 6-phosphate, 2-kinase : fructose 2,6-bisphosphatase. *Protein Science* **5**, 904–913.
17. Istvan, E.S., Hasemann, C.A., Kurumbail, R.G., Uyeda, K. & Deisenhofer, J. (1995). Crystallization and preliminary X-ray analysis of fructose 6-phosphate, 2-kinase:fructose 2,6-bisphosphatase. *Protein Sci.* **4**, 2439–2441.
18. Kurland, I.J., Chapman, B., Lee, Y.H. & Pilkis, S.J. (1995). Evolutionary reengineering of the phosphofructokinase active site: Arg-104 does not stabilize the transition state in 6-phosphofructo-2-kinase. *Biochem. Biophys. Res. Commun.* **213**, 663–672.
19. Li, L., Lin, K., Kurland, I.J., Correia, J.J. & Pilkis, S.J. (1992). Site-directed mutagenesis in rat liver 6-phosphofructo-2-kinase. Mutation at the fructose-6-phosphate binding site affects phosphate activation. *J. Biol. Chem.* **267**, 4386–4393.
20. Rider, M.H., Crepin, K.M., De Cloedt, M., Bertrand, L. & Hue, L. (1994). Site-directed mutagenesis of rat muscle 6-phosphofructo-2-kinase/fructose-2,6-bisphosphatase: role of Asp-130 in the 2-kinase domain. *Biochem. J.* **300**, 111–115.

21. Tsujikawa, T., Watanabe, F. & Uyeda, K. (1995). Hexose phosphate binding sites of fructose 6-phosphate,2-kinase:fructose 2,6-bisphosphatase. *Biochemistry* **34**, 6389–6393.
22. Winn, S.I., Watson, H.C., Harkins, R.N. & Fothergill, L.A. (1981). Structure and activity of phosphoglycerate mutase. *Philos. Trans. R. Soc. Lond. [Biol.]* **293**, 121–130.
23. Schneider, G., Lindqvist, Y. & Vihko, P. (1993). Three-dimensional structure of rat acid phosphatase. *EMBO J.* **12**, 2609–2615.
24. Li, L., Lin, K., Correia, J.J. & Pilkis, S.J. (1992). Hepatic 6-phosphofructo-2-kinase/fructose-2,6-bisphosphatase. The role of surface loop basic residues in substrate binding to the fructose-2,6-bisphosphatase domain. *J. Biol. Chem.* **267**, 21588–21594.
25. Li, L., Lin, K., Correia, J.J. & Pilkis, S.J. (1992). Lysine 356 is a critical residue for binding the C-6 phospho group of fructose-2,6-bisphosphate to the fructose-2,6-bisphosphatase domain of rat liver 6-phosphofructo-2-kinase/ fructose-2,6-bisphosphatase. *J. Biol. Chem.* **267**, 16669–16675.
26. Tauler, A., Lin, K. & Pilkis, S.J. (1990). Hepatic 6-phosphofructo-2-kinase/ fructose-2,6-bisphosphatase. Use of site-directed mutagenesis to evaluate the roles of His-258 and His-392 in catalysis. *J. Biol. Chem.* **265**, 15617–15622.
27. Lin, K., Li, L., Correia, J.J. & Pilkis, S.J. (1992). Glu327 is part of a catalytic triad in rat liver fructose-2,6-bisphosphatase. *J. Biol. Chem.* **267**, 6556–6562.
28. Lin, K., Li, L., Correia, J.J. & Pilkis, S.J. (1992). Arg257 and Arg307 of 6-phosphofructo-2-kinase/fructose-2,6-bisphosphatase bind the C-2 phospho group of fructose-2,6-bisphosphate in the fructose-2,6-bisphosphatase domain. *J. Biol. Chem.* **267**, 19163–19171.
29. Walker, J.E., Saraste, M., Runswick, M.J. & Gay, N.J. (1982). Distantly related sequences in the α- and β-subunits of ATP synthase, myosin, kinases and other ATP-requiring enzymes and a common nucleotide binding fold. *EMBO J.* **1**, 945–951.
30. Schulz, G.E. (1992). Binding of nucleotides by proteins. *Curr. Opin. Struct. Biol.* **2**, 61–67.
31. Kurland, I.J., Li, L., Lange, A.J., Correia, J.J., El-Maghrabi, M.R. & Pilkis, S.J. (1993). Regulation of rat 6-phosphofructo-2-kinase/fructose-2,6-bisphosphatase. Role of the NH2-terminal region. *J. Biol. Chem.* **268**, 14056–14064.
32. Lin, K., *et al*., & Pilkis, S.J. (1994). Evidence for NH_2- and COOH-terminal interactions in rat 6-phosphofructo-2-kinase/fructose-2,6-bisphosphatase. *J. Biol. Chem.* **269**, 16953–16960.
33. Kurland, I.J. & Pilkis, S.J. (1995). Covalent control of 6-phosphofructo-2-kinase/ fructose-2,6-bisphosphatase: insights into autoregulation of a bifunctional enzyme. *Protein Sci.* **4**, 1023–1037.
34. Fothergill-Gilmore, L.A. & Watson, H.C. (1989). The phosphoglycerate mutases. *Adv. Enzymol*. **62**, 227–313.
35. Bodansky, O. (1972). Acid phosphatase. *Adv. Clin Chem*. **15**, 43–147.
36. Rose, Z.B. (1970). Evidence for a phosphohistidine protein intermediate in the phosphoglycerate mutase reaction. *Arch. Biochem. Biophys*. **140**, 508–513.
37. Van Etten, R.L. (1977). Phosphohistidine as a stoichiometric intermediate in reactions catalyzed by isoenzymes of wheat germ acid phosphatase. *Arch. Biochem. Biophys*. **183**, 250–259.
38. Pilkis, S.J., *et al*., & El-Maghrabi, M.R. (1983). 6-Phosphofructo-2-kinase/ fructose 2,6-bisphosphatase from rat liver. *J. Biol. Chem.* **258**, 6135–6141.
39. Lee, Y.-H., *et al*., & Pilkis, S.J. (1996). Crystal structure of the rat liver fructose-2,6-bisphosphatase based on selenomethionine multiwavelength anomalous dispersion phases. *Biochemistry* **35**, 6010–6019.
40. Evans, P.R., Farrants, G.W. & Hudson, P.J. (1981). Phospho-fructokinase: structure and control. *Philos. Trans. R. Soc. Lond. [Biol.]* **293**, 53–62.
41. Müller, C.W. & Schulz, G.E. (1992). Structure of the complex between adenylate kinase from *Escherichia coli* and the inhibitor Ap5A refined at 1.9 Å resolution. *J. Mol. Biol.* **224**, 159–177.
42. Müller-Dieckmann, H.-J. & Schulz, G.E. (1995). Substrate specificity and assembly of the catalytic center derived from two structures of ligated uridylate kinase. *J. Mol. Biol.* **246**, 522–530.
43. Pai, E.F., Krengel, U., Petsko, G.A., Goody, R.S., Kabsch, W. & Wittinghofer, A. (1990). Refined crystal structure of the triphosphate conformation of H-ras p21 at 1.35 Å resolution: implications for the mechanism of GTP hydrolysis. *EMBO J.* **9**, 2351–2359.
44. Coleman, D.E., Berghuis, A.M., Lee, E., Linder, M.E., Gilman, A.G. & Sprang, S.R. (1994). Structures of active conformations of $G_{i\alpha 1}$ and the mechanism of GTP hydrolysis. *Science* **265**, 1405–1412.
45. Knowles, J.R. (1980). Enzyme-catalyzed phosphoryl transfer reactions. *Annu. Rev. Biochem*. **49**, 877–919.
46. Yoshida, M. & Amano, T. (1995). A common topology of proteins catalyzing ATP-triggered reactions. *FEBS Lett*. **359**, 1–5.
47. Admiraal, S.J. & Herschlag, D. (1996). Mapping the transition state for ATP hydrolysis - implications for enzymatic catalysis. *Chem. Biol*. **2**, 729–739.
48. Schulz, G.E., Müller, C.W. & Diederichs, K. (1990). Induced-fit movements in adenylate kinases. *J. Mol. Biol*. **213**, 627–630.
49. Müller, C.W., Schlauderer, G.J., Reinstein, J. & Schulz, G.E. (1996). Adenylate kinase motions during catalysis: an energetic counterweight balancing substrate binding. *Structure* **4**, 147–156.
50. Shirakihara, Y. & Evans, P.R. (1988). Crystal structure of the complex of phosphofructokinase from *Escherichia coli* with its reaction products. *J. Mol. Biol.* **204**, 973–994.
51. Steitz, T.A., Shoham, M. & Bennett, W.S., Jr. (1981). Structural dynamics of yeast hexokinase during catalysis. *Philos. Trans. R. Soc. Lond. [Biol.]* **293**, 43–52.
52. Joao, H.C. & Williams, R.J.P. (1993). The anatomy of a kinase and the control of phosphate transfer. *Eur. J. Biochem*. **216**, 1–18.
53. Levine, M., Muirhead, H., Stammers, D.K. & Stuart, D.I. (1978). Structure of pyruvate kinase and similarities with other enzymes: possible implications for protein taxonomy and evolution. *Nature* **271**, 626–630.
54. Kabsch, W. (1988). Evaluation of single-crystal X-ray diffraction data from a position sensitive detector. *J. Appl. Cryst*. **21**, 916–924.
55. Otwinowski, Z. & Minor, W. (1996). The HKL program suite. *Methods Enzymol*., in press.
56. Collaborative Computational Project, Number 4. (1994). The CCP4 suite: programs for protein crystallography. *Acta Crystallogr. D* **50**, 760–763.
57. Brünger, A.T. (1993). *X-PLOR Version 3.1: A System for Crystallography and NMR*. Yale University Press, New Haven, CT.
58. Jones, T.A., Zou, J.-Y., Cowan, S.W. & Kjeldgaard, M. (1991). Improved methods for building protein models in electron-density maps and the location of errors in these models. *Acta Cryst. A* **47**, 110–119.
59. Read, R.J. (1986). Improved Fourier coefficients for maps using phases from partial structures with errors. *Acta Cryst. A* **42**, 140–149.
60. Bernstein, F.C., *et al*., & Tasumi, M. (1977). The protein data bank: a computer-based archival file for macromolecular structures. *J. Mol. Biol.* **112**, 535–542.
61. Nicholls, A. & Honig, B. (1993). GRASP: graphical representation and analysis of surface properties, Columbia University, NY, USA.